Budget Friendly Flow Mapping: Utilizing Particle Streak Angles for Effective Turbulence Detection in Particulate Pipe Flow

R. Raj[1], A. Thiruthummal[1], A. Pothérat[1,*]

1: Centre for Fluids and Complex Systems, Coventry University
*Corresponding author: aa4111@coventry.ac.uk

Keywords: Pipe Flow, Streak angle, Flow visualization.

ABSTRACT

Comprehending the complexity of pipe flow dynamics is important for a variety of sectors, including environmental, industrial, and engineering research. Conventional techniques such as Particle Image Velocimetry (PIV) and Laser Doppler Velocimetry (LDV) have long been the heart of these kinds of investigations, but they are often quite expensive and complex. Our research offers a novel, affordable visualization method that aims to transform the way we examine and interpret flow dynamics in response to these challenges. Our method is developed to utilize a low-cost camera system with a simple laser setup to investigate fluid dynamics inside pipes. By introducing particles into the flow and manipulating the camera shutter speed in real-time under the laser, we created streaks capable of displaying complex flow patterns. We gathered precise information about streak angles using rigorous image processing, providing clarity in our insights into the flow dynamics of the particulate pipe flow. Notably, our strategy eliminates the need for expensive and sophisticated equipment while providing researchers and practitioners with a simple yet reliable alternative. The potential for improving our knowledge of pipe flow dynamics is shown by preliminary studies that demonstrate how well it captures dynamic flow characteristics. Our technique, which is easy to use and effective, promises fresh insights into fluid dynamics and opens up new avenues for pipe flow analysis, making it suitable for a broad spectrum of users.

1. Introduction

Pipe flow presents a unique scenario in fluid dynamics due to its ability to remain laminar across a range of Reynolds numbers. Essentially, minute disturbances in the flow dissipate over time, mandating specific conditions for transitioning to instability (Salwen & Grosch, 1972; Salwen et al., 1980). The transition from laminar to turbulent states occurs as the Reynolds number (Re) increases, marked by the spontaneous emergence of eddies disrupting the laminar flow. These disruptions manifest as 'puffs' and 'slugs,' localized turbulent regions within an otherwise laminar flow, characterized by chaotic velocity fluctuations (Mullin & Peixinho, 2006; Eckhardt et al., 2007; Nishi et al., 2008).

Experimental investigations into pipe flow stability demand a precisely controlled flow setup to ensure disturbance-free conditions across a wide range of Reynolds numbers (Fargie & Martin, 1971). Achieving this involves careful design considerations, such as employing smooth funnel-like inlets to minimize flow perturbations (Bandyopadhyay, 1986; Darbyshire & Mullin, 1995). Utilizing displacement devices resembling large syringes allows for precise control of mass flux and Reynolds number (Darbyshire & Mullin, 1995; Peixinho & Mullin, 2007).

Once the experimental rig is established, visualization techniques become essential for gaining insights into fluid behaviors. Traditional methods like dye injection, particle tracking, and smoke visualization aid in observing flow patterns and understanding fundamental fluid dynamics principles (Settles, 1986; Smits, 2012). However, for studying complex fluid dynamics, especially in low particle density two-phase pipe flows, advanced techniques such as Particle Image Velocimetry (PIV) and Laser Doppler Velocimetry (LDV) offer invaluable quantitative data on velocity distributions and phase interactions (Adrian, 1991; So et al., 2002; George & Lumley, 1973; Adrian & Westerweel, 2011; Wang, 1988).

Despite the benefits of PIV and LDV, their high costs, computational demands, and complexity limit their accessibility and widespread adoption, particularly in research settings with budget constraints (Adrian, 2005). Hence, there arises a need for a cost-effective, user-friendly, and reliable method to study particulate pipe flow dynamics. The proposed technique aims to bridge these gaps by validating the proposed streak visualization method against established PIV and pressure drop techniques, offering a practical tool for detecting laminar, transitional, and turbulent flow states in particulate pipe flows.

In this paper, we present the development and validation of our novel approach for studying particulate pipe flow dynamics. We detail the experimental setup, methodology, and results obtained from preliminary tests, highlighting the potential of our technique in advancing the field of fluid dynamics research. Through our contributions, we aim to stimulate further innovation and exploration in the study of particle-laden flows.

2. Experimental Setup

The experimental setup is an upgrade of the setup described in detail in (Singh et al., 2020). It consists of several subsystems, all represented on section 1. The pipe and hydraulic elements form the main component, through which the fluid and the particles travel. The glass pipe assembly comprises 10 cylindrical borosilicate glass tubes, each 1.2m long, with a bell mouth inlet and an additional 25 cm glass section towards the flow exit. The pipe dimensions are precise, with lengths of 1.2m $\pm$ 10-30 μm, an inner bore diameter of 20 mm $\pm$ 0.1 mm, and a wall thickness of 3.1 mm $\pm$ 0. This setup was designed to experimentally study the effects of solid, neutrally buoyant, spherical particles on the transition to turbulence in dilute particle-laden pipe flows.

The first upgrade to the original system is a change of working fluid, tracers, and particles that

makes the rig now operable with practically just water and a bit of glycerol (mixture ratio $\approx 63:1$), *i.e.*, much simpler to operate than the aqueous solution of Sodium Polytungstate that was initially chosen to match the density ($2500\,\mathrm{kg/m^3}$) of glass particles used to seed it. This change was made possible by the availability of opaque polyethylene particles of density close to that of water. Indeed, two types of particles are required to study particulate flows: the first ones are tiny silver-coated hollow glass particles (in size range of $10\,\mu$m) that follow the flow almost instantaneously and are used for Particle Image Velocimetry, and are referred to as tracers. To act like tracers, the particles' response time needs to be much smaller than the time scale of the flow, or the Stokes number value(St) should be $\ll 1$. In our experiments, the Stokes number is within the range $[7\times10^{-6}, 2\times10^{-4}]$, fulfilling the criterion.

The second type of particles, on the other hand, are much larger particles (of St close to 1) , alter the dynamics of the fluid phase, and are used to study the particulate flow dynamics that result from the interaction between those two phases. The working fluid consists of a mixture of water and glycerol, where glycerol is added to achieve neutral buoyancy with the particles under study. This adjustment results in a fluid density (ρ_f) of $1,000\,\mathrm{kg/m^3}$, composed of 98.4% water and 1.6% glycerol. Two diameter ranges of particles are utilized: the first type has diameters ranging from $425\,\mu$m to $500\,\mu$m, while the second type ranges from $212\,\mu$m to $250\,\mu$m. The particle-to-pipe volume ratios are respectively between $[0.0212, 0.025]$ and $[0.0106, 0.0125]$. The particle concentration during experiments is $C = 1.2\,\mathrm{kg/m^3}$ for the experiments, corresponding to a volume fraction of $\Phi = 1.2\times10^{-3}$.

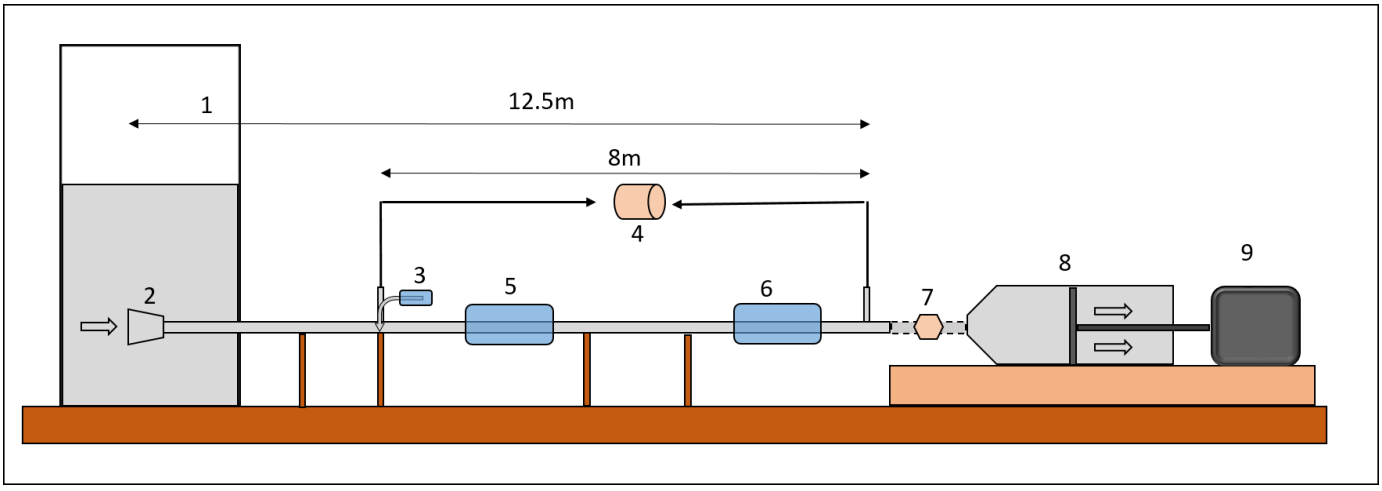

Figure 1. A 2-D schematic diagram of the rig. (1) Fluid Reservoir, (2) Bell-mouth inlet,(3) Perturbation system, (4) Differential pressure meter, (5) 1^{st} visualization system, (6) 2^{nd} visualization system, (7) Mass flow meter, (8) Piston-cylinder arrangement, (9) Motor

Upstream of the pipe, the system has a reservoir at one end, where the fluid is stored. A bell mouth inlet placed inside this reservoir allows a smooth entry of the fluid into the pipe. The other end of the pipe is connected to a piston-cylinder arrangement driven by a motor. The fluid from the reservoir is pulled through the pipe when this motor pulls the piston, thus creating a pressure

difference and driving the fluid.

The second subsystem is aimed at introducing precisely controlled velocity perturbation perpendicular to the mean flow. This perturbation subsystem is made of a syringe and a stepper motor, connected to the main pipe at 4.5m downstream of the inlet. The stepper motor is controlled by an Arduino that sets the volume and flow rate of the injected perturbation. The effect of the introduced perturbation on the fluid-particle system is visualized at two downstream locations by two different measurement systems. The 1st visualization system consists of a powerful laser and a high-speed camera used for simultaneous Particle Tracking Velocimetry (PTV) and Particle Image Velocimetry (PIV). The purpose of this system is to independently and simultaneously track large particles and map flow velocities by PIV in a vertical plane aligned with the pipe axis, lit by the laser. The details of this technique can be found in (Singh et al., 2020). The 2nd visualization system is the newly developed streak visualization system and is positioned 4.45 meters downstream from the first, PTV/PIV visualization system.

Fig. 2 shows a 2-D lateral view of the streak visualization setup and the image of the actual setup placed in the rig. The visualization systems employ a basic 50 mW laser, and a low-cost Flea camera (Blackfly-FLIR). The camera's resolution is set to 1536 x 2048 pixels, and it is equipped with a 35 mm focal length lens. The gain has been adjusted to prevent excessive brightness. This technique offers a simple means of understanding and analyzing the flow behavior within the pipe.

The opaque particles, introduced into the fluid under examination, reflect the laser light sheet. The camera is oriented perpendicular to the laser sheet, and captures images with adjusted shutter speed varying from 15 ms to 50 ms, for the different value of the Reynolds number Re. This camera setting was chosen to ensure that the captured images depict the particles as distinct streaks of light, thus providing a visual representation of the angles subtended by the path of the particles, with respect to the pipe axis.

The rationale for capturing streaks lies in the distinct characteristics exhibited in laminar and turbulent fluid flows. In laminar conditions, the streaks are anticipated to align parallel to the mean flow direction, whereas in turbulent scenarios, the streaks are expected to be oriented in a more random manner. The purpose of this paper is to show that this methodology is particularly insightful in transitional flow regimes, as it enables the identification of turbulent patches occurring intermittently within the overarching laminar flow.

Lastly, The test rig was also fitted with a high-speed differential pressure transducer (Omega USBH Series). It is a USB-based device and comes with its own software for direct recording in the computer. It has a range of 0 to 70 mbar, with an accuracy of $\pm 0.08\%$ and a sampling frequency of 1000 readings/second.

The differential pressure is measured across the pipe from the point of injection of disturbance till the pipe's end section over a distance of 8.3 m. To accomplish this an extra 20 cm glass section with a T-inlet was manufactured separately and connected at the end of the pipe, thus enabling the differential pressure meter to be connected at the end of the pipe section.

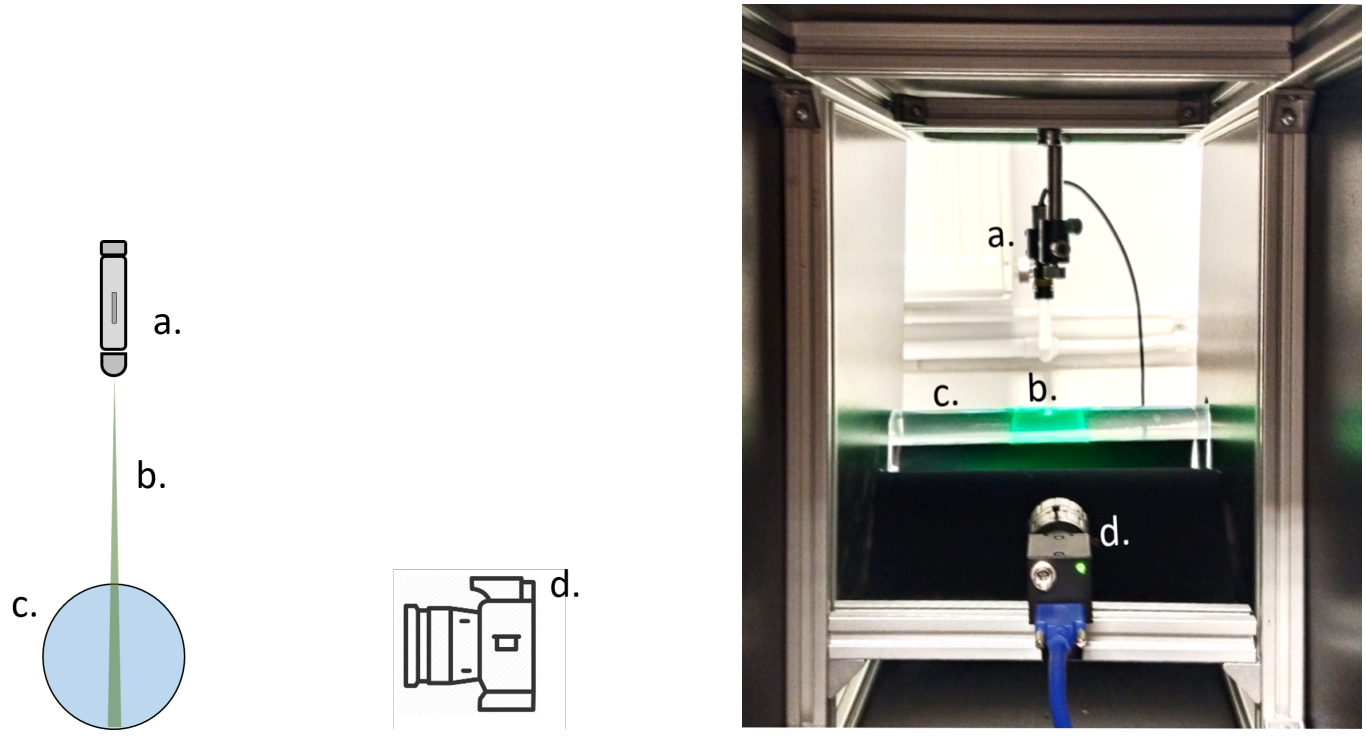

(a) 2-D diagram of the lateral view of streak visualization setup

(b) Actual image of the setup

Figure 2. Sketch and picture of the second visualization system for streak-angle velocimetry. In both instances, (a) is the laser, (b) is the laser sheet produced, (c) is the glass pipe, and (d) is the camera lens setup

2.1. Experimental control parameters

- Reynolds number (Re) ranging from 1120 to 2980,
- Particle-to-fluid volume fraction (Φ) of 1.2×10^{-3},
- Particle diameters of $425\,\mu$m $-$ $500\,\mu$m and $212\,\mu$m $-$ $250\,\mu$m,
- Perturbation volumes of 0.5 ml and 1 ml, applied for 90 ms.

These parameters were chosen to comprehensively study the effects of different flow regimes, particle sizes, and perturbation magnitudes on the behavior of particles in a fluid flow.

2.2. Experimental procedure

Before running the experiment, the fluid was mixed by driving back and forth the flow in the pipe to ensure the homogeneity of the particles and the tracers in the fluid. This process was also used to eject any bubbles present in the pipe. After each experiment, an idle time of approximately 25 minutes was needed to allow the fluid to become steady.

The motor was run at a specific rpm to achieve the required Re for the fluid. Once the flow started, the perturbation was introduced into the system, and data acquisition for the pressure drop system

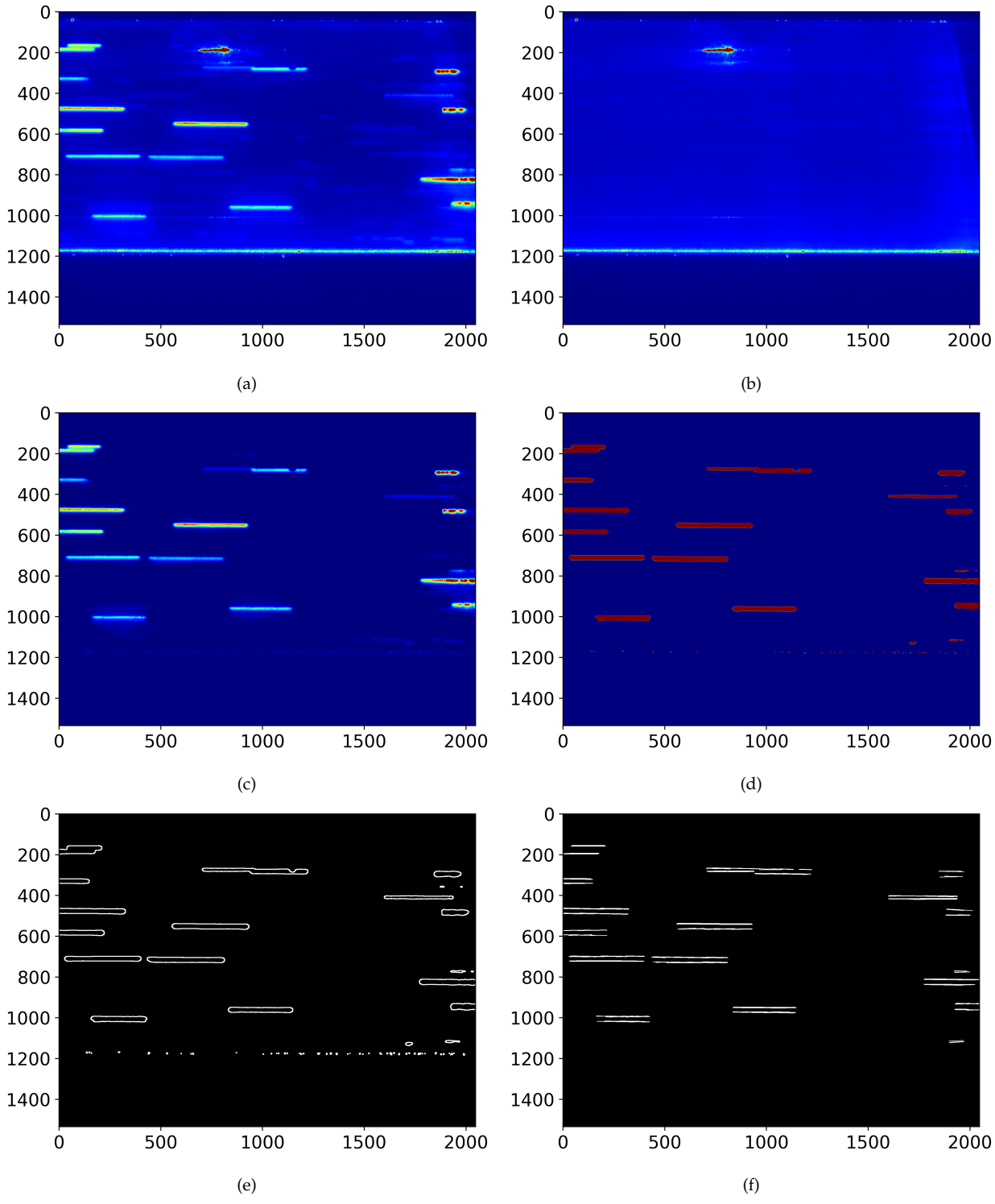

Figure 3. Successive stages of image processing for the streak-angle velocimetry. The horizontal and vertical axes represent values in pixels. (a) Raw image, (b) background frame, (c) image after background subtraction, (d) image after adaptive thresholding, (e) image after canny edge detection and (f) Lines detected by Hough transform (showing the two lines per actual streak).

was simultaneously initiated. Images were captured by the 1st visualization system for simultaneous PTV/PIV processing. The timing of these image captures was coordinated to ensure that the

perturbation was captured, with its velocity estimated based on the fluid velocity.

Subsequently, images were captured by the 2nd visualization system for streak visualization analysis, timed based on the estimated arrival of the perturbation at this system. The acquired images were collected for processing. These experiments were repeated six times for each case to ensure the reliability and accuracy of the data.

3. Image Processing for the streak visualization systems

The image processing was performed using OpenCV library in Python (*OpenCV-Python: Open Source Computer Vision Library in Python*, 2023). The task here is to detect the lines corresponding to the streaks in the image and then extract the angles the lines make with the pipe axis. The raw image from the camera (Figure. 3a) contains various artifacts due to the reflection of light from the surface of the pipe. In order to remove these artifacts, a background frame (Figure. 3b) is constructed by averaging over all frames in each experimental run. This background frame is then subtracted from each of the raw images to obtain the background subtracted image (Figure. 3c). Once a cleaner artifact free image is obtained the next step is to identify the streaks, which involves applying a threshold to obtain a binary image with 1s and 0s corresponding to pixels which are part of the streak and background respectively. This is usually achieved through thresholding. In simple thresholding, a global threshold value is chosen and pixels with larger values are set to 1 and smaller values to 0. A simple thresholding doesn't work for our purpose due to uneven lighting and varying brightness of the streaks. Instead, an adaptive thresholding algorithm is used, where the threshold value is the mean of the pixel values in the neighborhood area minus a constant C. In this work, the neighborhood is chosen as a square with 101 pixels side length with the pixel of interest at its center and the constant C is chosen to be -8 in this study. In our experiments, the captured images have a bit depth of 8 bits, where each pixel can assume an integer value from 0 to 255 with 0 and 255 being the darkest and brightest respectively. The choice of adaptive thresholding parameters were made empirically for this specific experimental setup based on visualization as shown in Figure. 3d and will depend on the bit depth, sensitivity and resolution of the camera as well as the illumination used in the experimental setup. Note that for noisy or grainy images, it is preferable to apply a Gaussian smoothing prior to applying adaptive thresholding to reduce noise in the thresholded binary image.

In principle, a Hough transform (Hough, 1962; Duda & Hart, 1972) can now be utilized to detect lines from the binary image of streaks. However, owing to the non-negligible thickness of the streaks, multiple lines would be detected corresponding to the same steak if the Hough transform was applied directly to the binary images. This would skew the computed statistics since the number and angle of lines detected would depend on the thickness of the streaks. In order to mitigate this issue, we first use the Canny edge detection algorithm (Canny, 1986) to identify the edges (Figure. 3e) and then apply the Hough transform to extract the lines as shown in Figure. 3f. Even though this results in 2 lines being detected for most streaks, there won't be any appreciable ef-

fect on any statistical distribution of angle, which is the key information we are seeking to extract. The incorrect count can even be simply corrected with a division by 2. The Canny edge detection as implemented in OpenCV has different parameters including minimum threshold, maximum threshold, and aperture size. Here aperture size refers to the size of the matrix representing the derivative operation and will determine how many neighboring pixels are considered when computing the derivative. Since we are using a binary image, the results won't be sensitive to threshold values and we chose the minimum aperture size of 3.

As for Hough transform, we use a probabilistic variant (Matas et al., 2000), which speeds up computations significantly with a small trade-off in accuracy. The parameters for the OpenCV implementation are set as follows: distance resolution of 1 pixel, angle resolution of 1 degree, accumulator threshold of 30 votes, minimum line length of 30 pixels, and maximum line gap of 20 pixels.

4. Results

4.1. Overview of the results obtained from the PIV setup

The fluid transition behavior observed in the experiments conducted in a pipe flow setup, as depicted in Table 1, provides valuable insights into the flow behavior within the system. The table presents results obtained from the post-processed data acquired from the PIV measurement setup which is placed upstream of the streak visualization setup, showcasing the fluid response to different Re values. The results in the Table 1 are for the case of particulate flow (particles range: 212 μm - 250 μm), while 0.5ml perturbation was introduced in the flow, influencing the fluid behavior. Our results are in accordance with the findings of Hogendoorn et al. (2022), where, the Re_c (critical Reynolds number) was found to scale to ϵ^{-1} where $\epsilon = (d_p/D)^{\frac{1}{2}}\ (\phi)^{\frac{1}{6}}$, where $d_p$is diameter of the particle and D is the pipe diameter. For this particular case of ours, the ϵ range is $0.033 - 0.0515$, which shows transition around the same Re_c value as predicted in their paper *i.e* $Re_c \approx 2300$.

Table 1. Fluid transition behavior for the given cases. 'Lam' and 'Turb' mean laminar and turbulent flow, and 'Puff' is the turbulent patch inside an otherwise laminar flow. The cases presented here are for different Re numbers as indicated.(Results obtained from PIV setup)

Particle Size (μm)	Volume fraction Φ	1120	1530	1980	2260	2550	2980
212-250	1.2×10^{-3}	Lam	Lam	Puff	Turb	Turb	Turb

As shown in Table 1, for smaller Re values, represented by the 1120 and 1530 categories, laminar flow predominates, indicating orderly, streamlined motion within the fluid. However, as the particle size increases, a transition to turbulent flow becomes evident, particularly noticeable for Re 1980 and above. In these cases, turbulent patches ('Puff') appear within an otherwise laminar flow, signifying the onset of turbulence within the system. For Re exceeding 2260, turbulent flow dominates entirely, characterized by chaotic motion and mixing within the fluid.

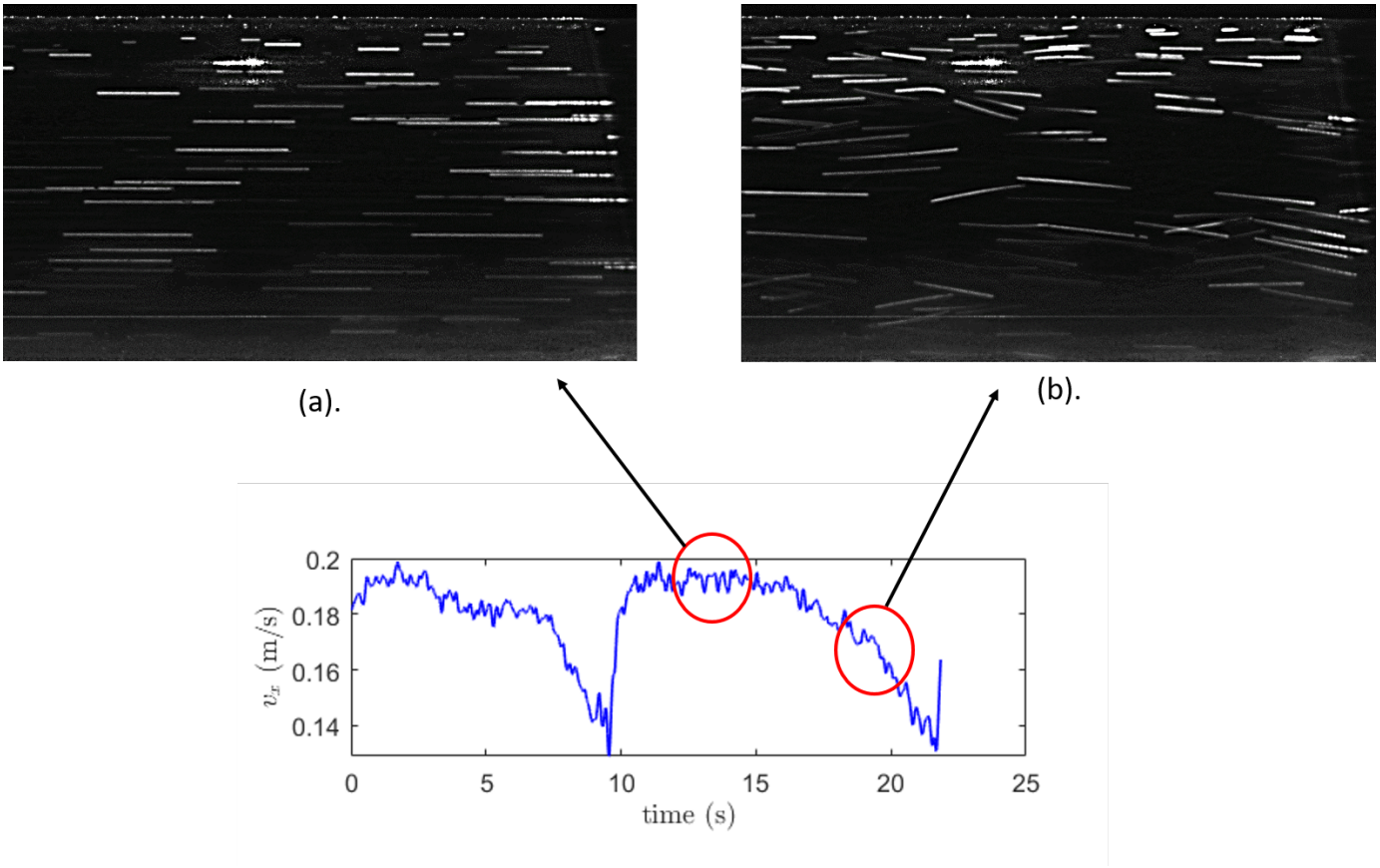

Figure 4. The blue line is the temporal centreline velocity of the fluid obtained from the PIV system at Re 1980 showing the passing of two puffs. The two images (a and b) shown here are obtained directly from the camera of the streak visualization setup and show the streaks produced by the particles. Both the images were taken at Re 1980 but (a) is the part where the flow is laminar and (b) was captured when the turbulent puff was passing

The values presented in Table 1 serve as crucial validation point for our streak visualization setup, positioned downstream of the Particle Image Velocimetry (PIV) system. As the fluid dynamics captured by the PIV measurements directly influence the behavior of streaks in the flow, these validation points enable us to assess the accuracy and reliability of our streak visualization technique. Furthermore, we can confirm the consistency between experimental observations from PIV setup and streak setup findings.

The images (a and b), as depicted in Figure 4, were captured directly from the camera of the streak visualization setup, showcasing the streaks generated by the particles within the fluid flow. Both images were acquired at a Reynolds number (Re) of 1980. Image 4(a) corresponds to a segment of the flow characterized by laminar behavior, while image 4(b) captures the passage of a turbulent puff.

These images 4 (a and b) were approximately taken at positions indicated by red circles overlaid on the centerline velocity profile obtained from the PIV setup. This positioning highlights the variation in streak angles between the laminar and turbulent regions of the fluid flow. Specifically, the observed change in streak angle serves as a visual indicator of the dynamics of the flow hence

solidifying our method for further processing using these streak angles.

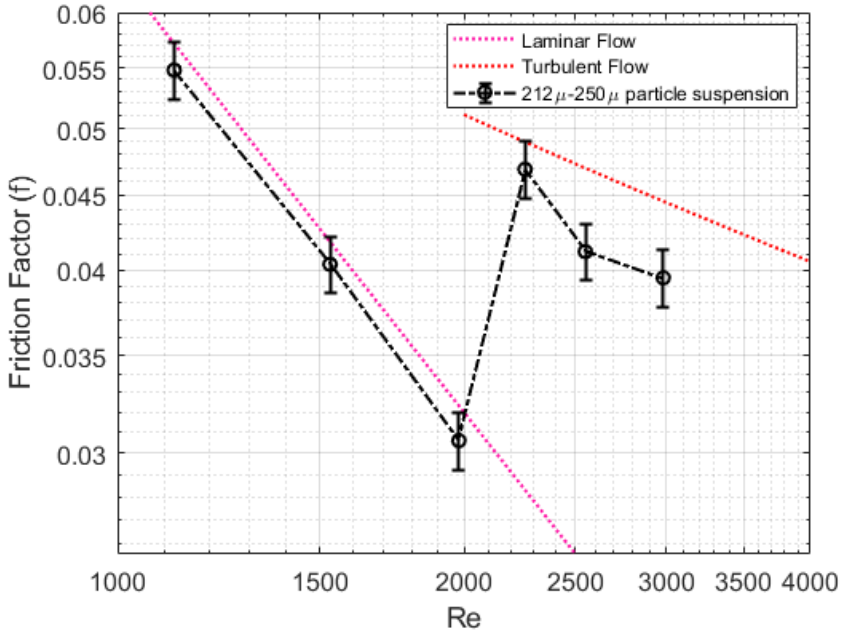

Figure 5. Friction factor vs Re based on the pressure drop readings obtained from the particulate pipe flow experiment against theoretical laminar and turbulent flows.

4.2. Utilization of Pressure Drop Measurements to Characterize Particulate Pipe Flow States

Next, we further address the question of knowing the overall flow state of the particle-fluid system, since visualizing particle streaks may only reflect the state of the fluid phase when both somewhat match. To do this, we use the the differential pressure meter to assess the pressure drop between the point where the perturbation is injected into the flow and the pipe's outlet. The pressure drop is controlled by the state of the fluid phase, and so offers a way to diagnose the turbulent or laminar state of the flow that is independent of the two visualization systems and crucially, regardless of how turbulent patches may evolve when traveling between the two systems. The experimental data containing pressure drop values of the fluid across the pipe was used to calculate the friction factor using the equation:

$$h_f = \frac{fLU^2}{2Dg} = \frac{\Delta P}{\rho g} \tag{1}$$

where h_f is the loss of head in friction, U is the mean velocity, g is the acceleration due to gravity, D is the diameter of the pipe, and ΔP is the pressure difference. The friction factor is a function of two dimensionless quantities: the Reynolds number (Re) and the relative roughness of the surface given by $\frac{E}{D}$ with E as the absolute roughness. In the laminar flow region, the friction factor is independent of roughness and follows the Hagen-Poiseuille law:

$$f_{\text{lam}} = \frac{64}{\text{Re}} \tag{2}$$

In contrast, in the turbulent flow region, the friction factor for a smooth pipe is described by the Kármán–Prandtl resistance equation:

$$\frac{1}{\sqrt{f}} = 1.930 \log\left(\frac{\mathrm{Re}}{\sqrt{f}}\right) - 0.537 \tag{3}$$

Refer to Figure 5 for the plot of the friction factor against the Reynolds number. Analysis of this plot allows the determination of the flow state based on the calculated friction factor. For Reynolds numbers of 1120 and 1530, the flow is laminar, indicated by the friction factor values in the plot. Even at Re $= 1980$, although the flow exhibits the presence of puffs detected by the Particle Image Velocimetry (PIV) system as discussed earlier, overall it remains within the laminar regime. However, for Reynolds numbers of 2260 and higher, the flow transitions to a turbulent regime, as evidenced by the friction factor values in the plot.

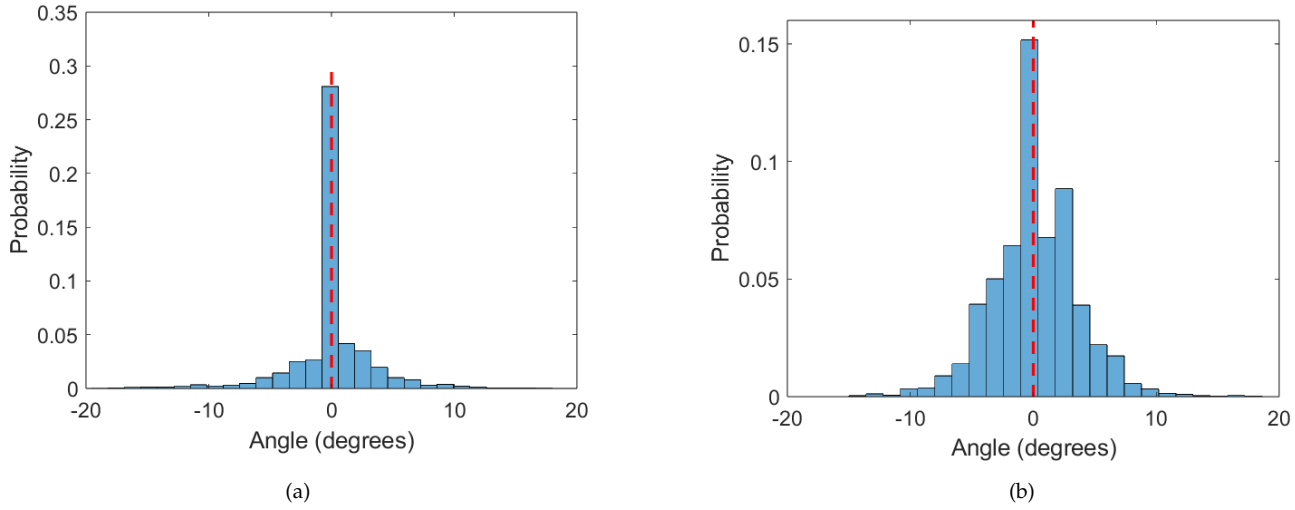

Figure 6. The depicted figures illustrate the probability distribution histograms of streak angles for two distinct Reynolds number scenarios. Figure (a) represents the streak angle distribution for the case with Re 1120, while Figure (b) portrays the streak angle distribution for the scenario with Re 2980.

By combining information from both the PIV system and the pressure drop measurements, the effectiveness of the streak visualization system could be evaluated and matched. Thus, the integration of the PIV and pressure drop system provided a comprehensive validation approach for the new system.

4.3. Flow behavior identification based on the standard deviation of streak angles

At first we plotted the binned probability distribution of angles for two typical cases. The result, illustrated in Fig. 6, demonstrates a clear disparity in the angle distributions between cases for two different Re numbers (Re 1120 and Re 2980). In the histogram representation, angles cluster towards zero degrees in laminar flows, signifying a more uniform directionality of particle streaks. Conversely, in relatively turbulent flows, the angle distribution is notably wider, reflecting the

chaotic nature of particle motion within the fluid. Hence we shall now attempt to infer flow patterns from the time variation of standard deviation of streak angles. However, to quantify the orientation of the streaks with sufficient statistical convergence, we consider the distribution of streak angles over multiple frames. In a single frame, there are multiple particles, each contributing a streak angle. Therefore, for each frame, there are multiple streak angles. The streak angles are collected for 5 consecutive frames. Then, the mean and standard deviation of these angles are calculated. Next, the data set is shifted by one frame, and the process is repeated. This means that the new set of 5 consecutive frames will include the previous 4 frames (excluding the first frame) and add the next frame in the sequence. Note that, increasing the number of frames used for computing the statistics will decrease the error and noise in the estimates but will decrease the temporal resolution of various features of interest. Decreasing the number of frames has the opposite effect. Hence, there is a trade-off between time resolution (which is improved by a higher sampling frequency, hence by reducing the number of successive frames used for the determination of the standard deviation) and statistical convergence. Denoting the set of streak angles obtained from 5 consecutive frames as $\{\theta_{i,i_n}\}$, where i varies from 1 to 5 denotes the frame and i_n denotes the streak angles in the i$^{\text{th}}$ frame. The standard deviation σ of these values measures the dispersion or spread of the angles around their mean value. Mathematically, the sample standard deviation σ is calculated as follows:

$$\sigma = \sqrt{\frac{\sum_{i=1}^{5}\sum_{i_n}(\theta_{i,i_n} - \bar{\theta}_i)^2}{\left(\sum_{i=1}^{5}\sum_{i_n} 1\right) - 1}} \tag{4}$$

where $\bar{\theta}$ is the mean of the set of angles $\{\theta_{i,i_n}\}$ given by:

$$\bar{\theta} = \frac{\sum_{i=1}^{5}\sum_{i_n}\theta_{i,i_n}}{\sum_{i=1}^{5}\sum_{i_n} 1} \tag{5}$$

A higher standard deviation σ indicates greater variability in the streak angles across the frames. When the fluid flow is laminar, the streak angles tend to align parallel to the reference axis (e.g., horizontal), resulting in a lower standard deviation. In contrast, turbulent flow leads to irregular and chaotic movement of particles, causing streaks with varying angles, resulting in a higher standard deviation.

We have analyzed the angles of streaks produced by particles in a fluid, focusing on their distribution characteristics under laminar and turbulent flow conditions. The angles of these streaks are indicative of the underlying flow properties, with laminar flows typically exhibiting narrower angle distributions tending towards zero degrees, while turbulent flows display broader and more spread-out distributions. Differentiating between the two cases is often easy by simply looking at the picture. There, are however cases where transitional features are difficult to differentiate. Hence, there is a need for a more systematic approach to the detection of patterns from pictures. The simplest approach to this problem is to imitate "human recognition" in its most basic form: when assessing whether streaks are mostly horizontally aligned or more randomly distributed, we assess an average distribution and its scattering, *i.e.* the standard deviation of the angles (the

average is always expected to be close to 0 provided there is a sufficiently large number of streaks in the picture considered).

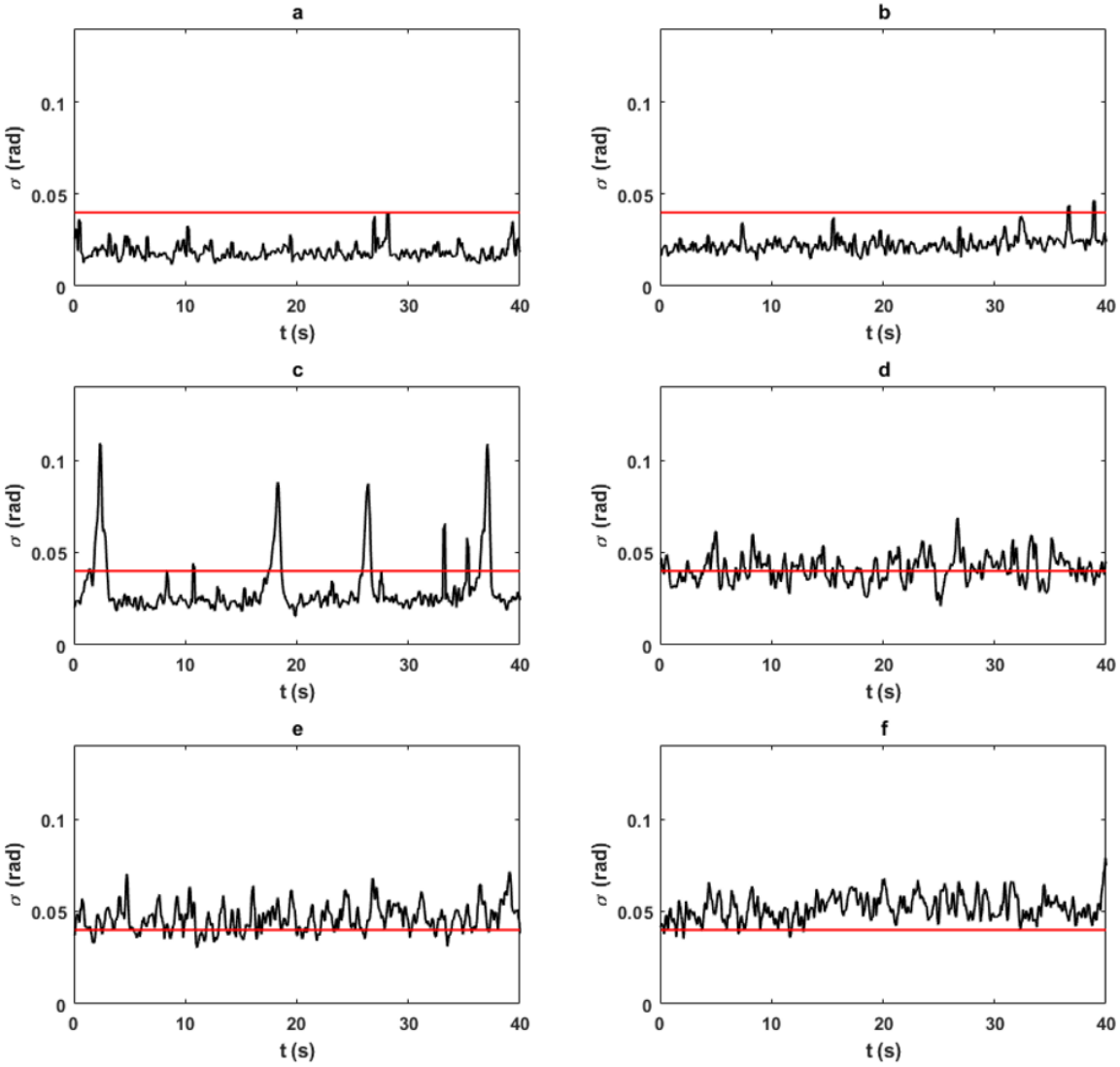

Figure 7. Variation of Standard Deviation over Time for Different Reynolds Numbers for fluid-particle mixture ($212\,\mu$m - $250\,\mu$m): Subfigures depict the temporal evolution of standard deviation values calculated from streak angles obtained through frame analysis for six different Reynolds numbers. The x-axis represents time(in seconds), while the y-axis represents the standard deviation (in radians) of streak angles. Subfigures (a) Re 1120, (b) Re 1530, (c) Re 1980, (d) Re 2260, (e) Re 2550 and (f) 2980 Additionally, a red line at the standard deviation value of 0.04 serves as a reference for distinguishing between laminar, transient, and turbulent flow regimes.

We first conducted repeated measurements under conditions of relatively high and low Reynolds numbers (Re 1100 and Re 7500), representing fully turbulent and fully laminar flows respectively to assess lower and upper bounds for the values of standard deviation. By plotting standard deviation values while simultaneously validating them with the PIV setup, a reference red line ($\sigma = 0.04$) separating both cases was established (as depicted in Fig. 7), serving as a benchmark for unknown cases. We also confirmed these results for each value of Re presented in Fig. 7 using

the PIV system and the pressure drop system as to further confirm the effectiveness of using the statistical distribution of streak angles in precisely understanding the flow characteristics.

The examination of subfigures under Figure 7 reveals more detailed information on the flow dynamics: For Figure 7(a) and (b) the flow was laminar (the standard deviation value throughout the time is well below the red line demarcation). As for the case within the transitional regime, found around Reynolds number 1980, shown in Figure 7(c), clear peaks of standard deviation peaks at certain places denoting the intermittent emergence of turbulent patches (puffs) amidst predominantly laminar flow conditions which was also observed by the PIV system. As the flow gradually transitions towards turbulence, exemplified by subfigure 7(d), standard deviation values progressively approach and eventually surpass the red line reference, indicating the onset of turbulent behavior. This transition becomes more pronounced in subfigures 7(e) and 7(f), where standard deviation values consistently exceed the red line, signifying fully turbulent flow conditions.

The outcomes of the flow analysis conducted with the pressure drop setup and the PIV system closely match the conclusions given by the proposed visualization system. From analysis and comparison of each subfigure under the reference plot shown in Figure 7, the supplementary data reinforces the identified trends in flow dynamics by the streak visualization method in not only identifying the nature of the flow but also detecting the presence of any transitional flow feature. Here, the identification of a simple threshold in the value of the standard deviation, calibrated from the purely laminar and purely turbulent state makes it possible to reliably detect transient features such as puffs.

5. Conclusions

In conclusion, the proposed streak visualization technique introduced in this research paper offers a promising path for cost-effective and efficient visualization of flow dynamics within the particulate pipe flow cases. Through effective pairing of a simple laser setup and an affordable camera system, this method enables real-time visualization of flow patterns by capturing streaks produced by particles present in the fluid.

Experimental validation, conducted through rigorous image processing and analysis, showcased the technique's effectiveness in capturing dynamic flow behaviors across a range of Reynolds numbers. The integration of complementary measurement systems, including Particle Image Velocimetry (PIV) and pressure drop analysis, further validated the authenticity and accuracy of the streak visualization results.

The presented findings highlight the method's ability to identify laminar, transitional, and turbulent flow regimes, providing valuable insights into flow characteristics with unprecedented clarity. Moreover, the technique's simplicity and affordability make it accessible to a wide range of interested parties.

It is however essential to acknowledge its limitations, which include its applicability being limited

to particulate flow cases, challenges in image processing for accurate streak angle determination, and the subjectivity and approximation involved in thresholding standard deviation for flow state determination.

Everything taken into consideration, the suggested streak visualization technique provides necessary insights into flow dynamics while still being affordable and easy to use. It is believed that more exploration and utilization of this approach will result in significant advances for both industrial and scholarly applications.

Acknowledgements

The authors would like to extend their gratitude to Ian Bates, lab technician at Coventry University, for his invaluable assistance. Special thanks to Lyse Brichet, intern (2022) and Mathilde Schneider, intern (2020–2021) from Ecole Normale Supérieure de Lyon, Université, for their contributions. Additionally, the authors acknowledge the fluids research group of Fluids and Complex Systems at Coventry University for their support and collaboration.

Nomenclature

Re	Reynolds number
Φ	Volume fraction
L	Length of the pipe [m]
U	Mean velocity [m/s]
g	Acceleration due to gravity [m/s^2]
D	Diameter of the pipe [m]
ΔP	Pressure difference [Pa]
h_f	Loss of head in friction [m]
f	Friction factor
E	Absolute roughness
σ	Standard deviation [radians]
θ	Streak angle [radians]

References

Adrian, R. J. (1991). Particle-imaging techniques for experimental fluid mechanics. *Annual review of fluid mechanics*, *23*(1), 261–304.

Adrian, R. J. (2005). Twenty years of particle image velocimetry. *Experiments in fluids*, *39*, 159–169.

Adrian, R. J., & Westerweel, J. (2011). *Particle image velocimetry* (No. 30). Cambridge university press.

Bandyopadhyay, P. R. (1986, 06). Review—Mean Flow in Turbulent Boundary Layers Disturbed to Alter Skin Friction. *Journal of Fluids Engineering*, *108*(2), 127-140. Retrieved from `https://doi.org/10.1115/1.3242552` doi: 10.1115/1.3242552

Canny, J. (1986). A computational approach to edge detection. *IEEE Transactions on pattern analysis and machine intelligence*(6), 679–698.

Darbyshire, A., & Mullin, T. (1995). Transition to turbulence in constant-mass-flux pipe flow. *Journal of Fluid Mechanics*, *289*, 83–114.

Duda, R. O., & Hart, P. E. (1972). Use of the hough transformation to detect lines and curves in pictures. *Communications of the ACM*, *15*(1), 11–15.

Eckhardt, B., Schneider, T. M., Hof, B., & Westerweel, J. (2007). Turbulence transition in pipe flow. *Annu. Rev. Fluid Mech.*, *39*, 447–468.

Fargie, D., & Martin, B. (1971). Developing laminar flow in a pipe of circular cross-section. *Proceedings of the Royal Society of London. A. Mathematical and Physical Sciences*, *321*(1547), 461–476.

George, W. K., & Lumley, J. L. (1973). The laser-doppler velocimeter and its application to the measurement of turbulence. *Journal of Fluid Mechanics*, *60*(2), 321–362.

Hogendoorn, W., Chandra, B., & Poelma, C. (2022). Onset of turbulence in particle-laden pipe flows. *Physical Review Fluids*, *7*(4), L042301.

Hough, P. V. (1962, December 18). *Method and means for recognizing complex patterns.* Google Patents. (US Patent 3,069,654)

Matas, J., Galambos, C., & Kittler, J. (2000). Robust detection of lines using the progressive probabilistic hough transform. *Computer vision and image understanding*, *78*(1), 119–137.

Mullin, T., & Peixinho, J. (2006). Recent observations of the transition to turbulence in a pipe. In *Iutam symposium on laminar-turbulent transition* (pp. 45–55).

Nishi, M., Ünsal, B., Durst, F., & Biswas, G. (2008). Laminar-to-turbulent transition of pipe flows through puffs and slugs. *Journal of Fluid Mechanics*, *614*, 425–446.

Opencv-python: Open source computer vision library in python. (2023). Retrieved from `https://github.com/opencv/opencv-python`

Peixinho, J., & Mullin, T. (2007). Finite-amplitude thresholds for transition in pipe flow. *Journal of Fluid Mechanics*, *582*, 169–178.

Salwen, H., Cotton, F. W., & Grosch, C. E. (1980). Linear stability of poiseuille flow in a circular pipe. *Journal of Fluid Mechanics*, *98*(2), 273–284.

Salwen, H., & Grosch, C. E. (1972). The stability of poiseuille flow in a pipe of circular cross-section. *Journal of Fluid Mechanics*, *54*(1), 93–112.

Settles, G. S. (1986). Modern developments in flow visualization. *AIAA journal*, *24*(8), 1313–1323.

Singh, S., Pothérat, A., Pringle, C. C., Bates, I. R., & Holdsworth, M. (2020). Simultaneous eulerian–lagrangian velocity measurements of particulate pipe flow in transitional regime. *Review of Scientific Instruments*, *91*(9).

Smits, A. J. (2012). *Flow visualization: techniques and examples*. World Scientific.

So, S., Morikita, H., Takagi, S., & Matsumoto, Y. (2002). Laser doppler velocimetry measurement of turbulent bubbly channel flow. *Experiments in Fluids*, *33*, 135–142.

Wang, C. P. (1988). Laser doppler velocimetry. *Journal of Quantitative Spectroscopy and Radiative Transfer*, *40*(3), 309–319.